Mobile Netw Appl (2017) 22:998–1009
DOI 10.1007/s11036-017-0820-2

A DOA Estimation Approach for Transmission Performance Guarantee in D2D Communication

Liangtian Wan[1] · Guangjie Han[1] · Jinfang Jiang[1] · Chunsheng Zhu[2] · Lei Shu[3]

Published online: 2 February 2017

Abstract In Device-to-Device (D2D) communications of massive Multiple-Input Multiple-Output (MIMO) system, the inter-channel interference (ICI) can severely deteriorate the entire system performance. The beamforming technique can be used to alleviate this situation. Thus the localization of the users' equipment (UE) should be known as a prior. In wireless communication, due to the effect of multipath, the model of incident signal should be regarded as distributed sources instead of point sources. In this paper, we propose a 2-D DOA estimation algorithm for coherently distributed (CD) sources based on conformal array. First, three rational invariance relationships are constructed based on generalized steering vectors (GSVs). Then the propagator method (PM) is used for estimating three rational invariance matrices. Finally, the 2-D DOA of CD sources can be obtained from the eigenvalues of three rational invariance matrices. Without spectrum peaking searching, and estimation and eigendecomposition of sampling covariance matrix, the proposed algorithm has low computational complexity. For the condition with a large amount of data, the distributed and parallel PM is proposed to deal with this problem. Simulation results verify the effectiveness of the proposed algorithm.

Keywords D2D communication · Conformal array · DOA estimation · CD sources · Propagator

✉ Guangjie Han
hanguangjie@gmail.com

Liangtian Wan
wanliangtian1@163.com

Jinfang Jiang
jiangjinfang1989@gmail.com

Chunsheng Zhu
cszhu@ece.ubc.ca

Lei Shu
lei.shu@ieee.org

[1] Department of Information and Communication Systems, Hohai University, Changzhou 213022, China

[2] Department of Electrical and Computer Engineering, The University of British Columbia, Vancouver, BC V6T 1Z4, Canada

[3] Guangdong Petrochemical Equipment Fault Diagnosis Key Laboratory, Guangdong University of Petrochemical Technology, Guangdong 525000, China

1 Introduction

In the era of mobile users' booming data, 4G cellular technologies can hardly meet the customers' demand. Thus researchers are seeking for new paradigms to revolutionize the traditional communication method of cellular networks [1]. Device-to-device (D2D) communication is one of such paradigms that appears to be a promising component in next generation cellular technologies, i.e., 5G. [2]. It enables user equipment (UE) to communicate directly with nearby other terminals over a D2D link without the help of cellular base stations (BS) [4]. Thus the energy efficient communication among different UE is very important to save the battery power of UEs [3]. Since the D2D link reuses the cellular frequency resource in underlay in-band D2D, the inter-channel interference (ICI) can severely

deteriorate the entire system performance [5]. In order to enhance transmission performance of D2D communication in massive MIMO system [6], the beamforming or interference cancellation techniques are used to guarantee the total system throughout [7]. The BS is equipped with a large number of antenna in massive MIMO system, such as uniform rectangular array (URA) and uniform cylindrical array (UCyA). This means that the beamforming should be implemented in both azimuth and elevation directions, i.e., three-dimensional (3-D) beamforming. The 3-D beamforming requires the position information of the UE, which corresponds to 2-D direction-of-arrival (DOA) of the UE. Conformal antenna (conformal array), which can be regarded as a more generalized form of URA and UCyA, is an antenna (an array) conformed to a surface whose shape is determined by considerations other than electromagnetic. The antenna installation is more flexible. However, the DOA estimation of conformal array is difficult because of its complex geometry structure. Thus the 2-D DOA estimation for 3-D beamforming in massive MIMO system via conformal array is a stubborn problem to solve.

In most applications of array processing, the point source model is adopted since the assumption that the signals come from narrow-band far-field is satisfied. In real applications, the effect of angular spread cannot be ignored because of the scattering, reflection, diffraction and refraction during the signal propagation. Thus the model of parameterized distributed source would be a good choice. The DOA estimation algorithm of point source is not suitable for CD source, or the performance would be degraded significantly. The distributed source model can be categorized into coherently distributed (CD) sources and incoherently distributed (ID) sources [8], which are corresponding to slowly time-varying channels and rapidly time-varying channels, respectively. For 1-D DOA estimation of CD source in massive MIMO system, the multiple signal classification (MUSIC) like approach has been proposed under the coexistence of circular and non-circular signals. For 2-D DOA estimation of ID source in massive MIMO system, the estimation parameter via rational invariance technique (ESPRIT) like approach has been proposed for URA [9] and UCyA [10], respectively. In addition, there are few reports about DOA estimation of CD sources based on conformal array as well. Thus in this paper, we aim to address the 2-D DOA estimation of CD source in massive MIMO system via conformal array.

Many DOA estimation algorithms [11] for CD sources have already been proposed [8, 12, 13]. These algorithms can be applied in wireless sensors network (WSN) with optimized rout [14]. However, the algorithms mentioned above can only deal with 1-D nominal DOA and angular extension estimation for CD sources, i.e., the array and the incident signals are in the same plane. In lots of real applications, it is more significant and valuable to estimate the 2-D DOA of CD sources. Traditional optimal estimators for 2-D DOA of CD sources need multidimensional parameter searching, which leads to high computational complexity. In order to reduce the computational cost, many algorithms have been proposed to deal with this problem. In [15], a sequential one-dimensional searching (SOS) algorithm has been proposed. A preliminary estimation result has been obtained via total least square-estimation parameter via rational invariance technique (TLS-ESPRIT) algorithm. Then two angular parameters can be estimated by sequential 1-D searching with reduced computational complexity. In [16], the quadric rotational invariance property (QRIP) has been presented for 2-D DOA estimation of CD sources based on two parallel ULAs. Without spectrum peaking searching, the decoupled of azimuth and elevation DOA has been achieved. In [17], based on three parallel ULAs, a modified propagator method has been used to estimate three rotational invariance matrices. The nominal angular parameters of CD sources contained in three rotational invariance matrices can be obtained without spectrum peaking searching. In [18], based on one-order Taylor approximation to the generalized steering vectors (GSVs), two rotational invariance matrices have been constructed. The ESPRIT has been used for nominal 2-D DOA estimation of CD sources with low computational complexity. In [19], the 3D matrix pencil method has been used for 2-D DOA estimation of CD sources. The algorithms in [15–19] all have low computational complexity. However, they are just suitable for planar array and cannot be applied to conformal array directly.

The conformal array has been studied in electromagnetics field [20], such as array design [21] and beamforming [22]. For DOA estimation of conformal array, several algorithms have already proposed as well. In [23], based on three rotational invariance matrices and parallel factor (PARAFAC) analysis theory, high accuracy frequency and DOA estimation for conformal array has been achieved. In [24], eight conformal antennas have been well designed first. In order to achieve high accuracy DOA estimation for non-circular sources, the 2-D non-circular multiple signal classification (NC-MUSIC) algorithm has been adopted. In [25], based on spctial mutual coupling matrix design and PARAFAC, the 2-D DOA and mutual coupling coefficients estimation have been achieved. In [26], the 2D DOA estimates are decoupled from polarization. The fourth-order cumulants of the array outputs and ESPRIT have been used for DOA estimation of conformal array. In [27], three rational invariance relationships have been constructed for cylindrical conformal array, then the propagator method has been used for DOA estimation.

In order to solve the DOA estimation of CD sources for conformal array, we propose a new algorithm to solve this problem. Based on the relationship among three generalized steering vectors (GSVs), we construct three rotational invariance matrices. The information of nominal azimuth and elevation is contained in the complex angle of the eigenvalues of three matrices mentioned above. Then a modified propagator method (PM) is proposed to estimate the DOA of CD sources. Compared with the MUSIC-based and ESPRIT-based algorithms, the spectrum peaking searching and eigenvalue decomposition of sampling covariance matrix are not needed, which means that the proposed algorithm has low computational complexity.

Notation In this paper, the operator $(\cdot)^{\#}$, $(\cdot)^{*}$, $(\cdot)^{\mathrm{T}}$, $(\cdot)^{\mathrm{H}}$ and $E\{\cdot\}$ are matrix pseudo-inverse, conjugate, transpose, conjugate transpose and expectation, respectively. The boldface uppercase letters and boldface lowercase letters denote matrices and column vectors, respectively. The symbol $\mathrm{diag}\{z_1, z_2\}$ stands for a diagonal matrix whose diagonal entries are z_1 and z_2, respectively. angle$(\cdot)$ is the phase operator of complex numbers, in radian.

The rest of paper is organized as follows. Section 2 gives the snapshot data model of conformal array for CD sources. Section 3 presents the modified propagator method for DOA estimation. The distributed and parallel scheme for DOA estimation with a large amount of data is constructed in Section 4. The computational complexity analysis is discussed in Section 5. Numerical results are given in Section 6, and the conclusions are drawn in Section 7.

2 Snapshot data model

When the elements are sheltered by the carrier, some elements cannot receive signals or the amplitude of the received signals is too weak. The SDT proposed in [12] is adopted in this paper, and we use three arrays to cover the whole space. The cylindrical conformal array has the characteristic of single curvature and symmetry, thus the structures of three arrays are identical. The methods of estimating DOA of the incident signals are identical as well. We just design and verify the algorithm for array 1. The DOA estimation of the whole space is based on the integration of the three arrays. As shown in Fig. 1a, the element-spacing in the same plane is $\lambda/4$; the distance between two neighboring planes is $\lambda/4$; the radius of the cylinder is 5λ, where λ is the wavelength of the incident signal. The direction vector of the incident signal $\mathbf{u}$ is shown in Fig. 1b.

2.1 Design of sub-arrays

The array structure used in this paper is shown in Fig. 1a. The elements numbered from 1 to m construct sub-array 1; the elements numbered from 2 to $m+1$ construct sub-array 2; the elements numbered from $m+3$ to $2m+2$ construct sub-array 3; the elements numbered from $2m+4$ to $3m+3$ construct sub-array 4. As shown in Fig. 2, the first sub-array pairing consists of sub-array 1 and sub-array 2, the distance vector between them is $\Delta\mathbf{P}_1$, which satisfies $d_1 = |\Delta\mathbf{P}_1| = \lambda/4$; the second sub-array paring consists of sub-array 1 and sub-array 3, the distance vector between them is $\Delta\mathbf{P}_2$, which satisfies $d_2 = |\Delta\mathbf{P}_2| = \lambda/4$; the third sub-array paring consists of sub-array 1 and sub-array 4, the distance vector between them is $\Delta\mathbf{P}_3$, which satisfies $d_3 = |\Delta\mathbf{P}_3| = \lambda/4$.

2.2 Snapshot data model

Assume D narrow far-field CD sources impinge on the conformal array as shown in Fig. 1a. The signals are

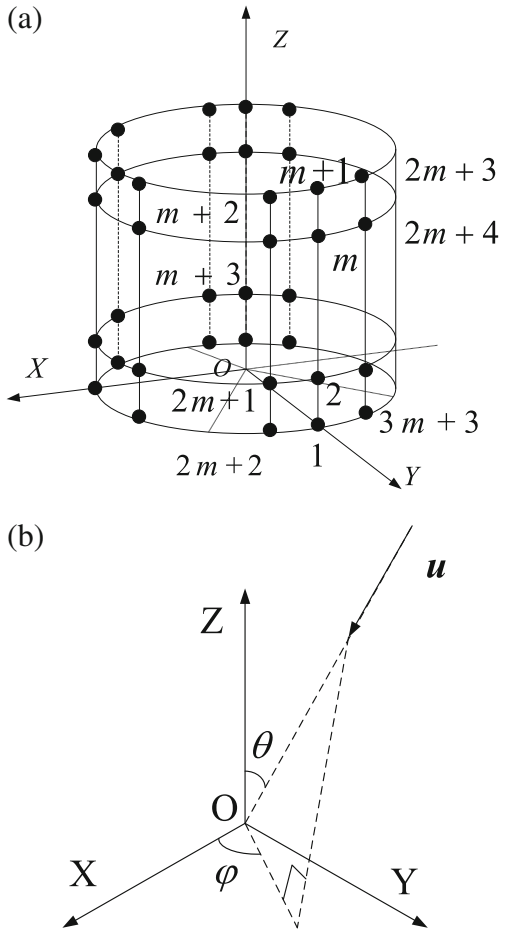

Fig. 1 The RMSE versus snapshot number

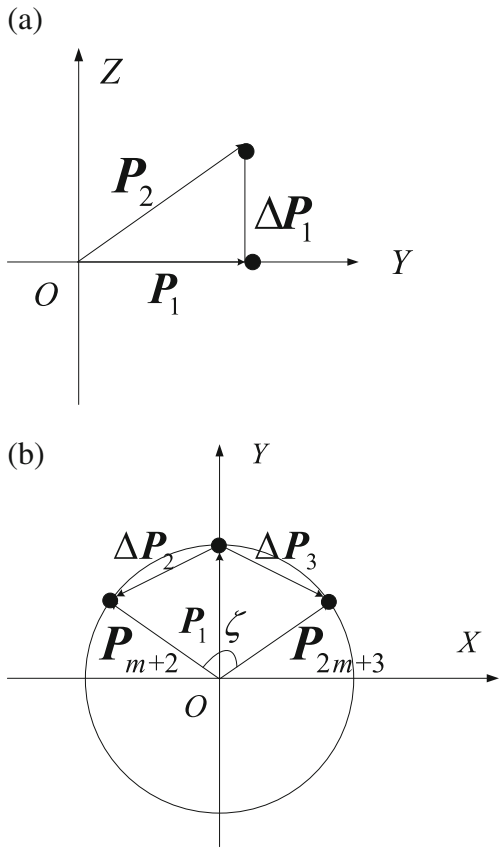

Fig. 2 The schematic diagram of distance vector among different sub-arrays

uncorrelated with each other, and the signals are uncorrelated with the additive Gaussian white noise (AGWN), which exists in each element.

For 2-D distributed sources, the received data $\mathbf{X}_1(t)$, $\mathbf{X}_2(t)$, $\mathbf{X}_3(t)$ and $\mathbf{X}_4(t)$ corresponding to sub-array 1, sub-array 2, sub-array 3 and sub-array 4 can be respectively expressed as

$$\mathbf{X}_1(t) = \sum_{i=1}^{D} \int\int \mathbf{a}(\theta,\varphi)\, s_i(t)\, \rho_i\left(\theta,\varphi;\boldsymbol{\mu}_i\right) d\theta d\varphi + \mathbf{N}_1(t), \tag{1}$$

$$\mathbf{X}_2(t) = \sum_{i=1}^{D} \int\int \mathbf{a}(\theta,\varphi) \exp(-j\omega_{1i})\, s_i(t) \times \rho_i\left(\theta,\varphi;\boldsymbol{\mu}_i\right) d\theta d\varphi + \mathbf{N}_2(t), \tag{2}$$

$$\mathbf{X}_3(t) = \sum_{i=1}^{D} \int\int \mathbf{a}(\theta,\varphi) \exp(-j\omega_{2i})\, s_i(t) \times \rho_i\left(\theta,\varphi;\boldsymbol{\mu}_i\right) d\theta d\varphi + \mathbf{N}_3(t), \tag{3}$$

$$\mathbf{X}_4(t) = \sum_{i=1}^{D} \int\int \mathbf{a}(\theta,\varphi) \exp(-j\omega_{3i})\, s_i(t) \times \rho_i\left(\theta,\varphi;\boldsymbol{\mu}_i\right) d\theta d\varphi + \mathbf{N}_4(t), \tag{4}$$

where $s_i(t)$ is the ith transmitted signal, $\rho_i\left(\theta,\varphi;\boldsymbol{\mu}_i\right)$ is a deterministic angular distribution function of the ith transmitted signal, $\boldsymbol{\mu}_i = \left(\theta_i, \sigma_{\theta_i}, \varphi_i, \sigma_{\varphi_i}\right)$, which corresponding to nominal azimuth DOA, azimuth angular extension, nominal elevation DOA and elevation angular extension, respectively, is the distributed parameter of the ith transmitted signal. $\mathbf{N}_1(t)$, $\mathbf{N}_2(t)$, $\mathbf{N}_3(t)$ and $\mathbf{N}_4(t)$ are the $M \times 1$ noise vector.

The steering vector of sub-array 1 can be expressed as

$$\mathbf{a}(\theta,\varphi) = \left[h_1 \exp\left(-j2\pi \frac{\mathbf{p}_1 \cdot \mathbf{u}}{\lambda}\right), \ldots, h_m \exp\left(-j2\pi \frac{\mathbf{p}_m \cdot \mathbf{u}}{\lambda}\right)\right]^T, \tag{5}$$

where the response of the ith element is

$$\begin{aligned} h_i &= \left(g_{i\theta}^2 + g_{i\varphi}^2\right)^{1/2} \left(k_\theta^2 + k_\varphi^2\right)^{1/2} \cos\left(\theta_{igk}\right) \\ &= |g_i|\,|q_l| \cos\left(\theta_{igk}\right) \\ &= \mathbf{g}_i \cdot \mathbf{q}_l = g_{i\theta} k_\theta + g_{i\varphi} k_\varphi. \end{aligned} \tag{6}$$

In (5), $\mathbf{p}_i$ is the position vector of the ith element. k_θ and k_φ are two polarization parameters, $\mathbf{g}_i$ is the pattern vector of the ith element, $\mathbf{q}_l$ is the electric field vector of the incident signal, the angle between the pattern vector and electric field vector is θ_{igk}. The frequency ω_{1i}, ω_{2i} and ω_{3i} can be respectively expressed as

$$\begin{aligned} \omega_{1i} &= \left(2\pi / \lambda_i\right) d_1 \Delta\mathbf{P}_1 \cdot \mathbf{u}_i \\ &= \left(2\pi d_1 / \lambda_i\right) [\sin\left(\theta_{\Delta\mathbf{P}_1}\right) \cos\left(\varphi_{\Delta\mathbf{P}_1}\right) \sin(\theta_i) \\ &\quad \times \cos(\varphi_i) + \sin\left(\theta_{\Delta\mathbf{P}_1}\right) \sin\left(\varphi_{\Delta\mathbf{P}_1}\right) \sin(\theta_i) \\ &\quad \times \sin(\varphi_i) + \cos\left(\theta_{\Delta\mathbf{P}_1}\right) \cos(\theta_i)], \end{aligned} \tag{7}$$

$$\begin{aligned} \omega_{2i} &= \left(2\pi / \lambda_i\right) d_2 \Delta\mathbf{P}_2 \cdot \mathbf{u}_i \\ &= \left(2\pi d_2 / \lambda_i\right) [\sin\left(\theta_{\Delta\mathbf{P}_2}\right) \cos\left(\varphi_{\Delta\mathbf{P}_2}\right) \sin(\theta_i) \\ &\quad \times \cos(\varphi_i) + \sin\left(\theta_{\Delta\mathbf{P}_2}\right) \sin\left(\varphi_{\Delta\mathbf{P}_2}\right) \sin(\theta_i) \\ &\quad \times \sin(\varphi_i) + \cos\left(\theta_{\Delta\mathbf{P}_2}\right) \cos(\theta_i)], \end{aligned} \tag{8}$$

$$\begin{aligned} \omega_{3i} &= \left(2\pi / \lambda_i\right) d_3 \Delta\mathbf{P}_3 \cdot \mathbf{u}_i \\ &= \left(2\pi d_3 / \lambda_i\right) [\sin\left(\theta_{\Delta\mathbf{P}_3}\right) \cos\left(\varphi_{\Delta\mathbf{P}_3}\right) \sin(\theta_i) \\ &\quad \times \cos(\varphi_i) + \sin\left(\theta_{\Delta\mathbf{P}_3}\right) \sin\left(\varphi_{\Delta\mathbf{P}_3}\right) \sin(\theta_i) \\ &\quad \times \sin(\varphi_i) + \cos\left(\theta_{\Delta\mathbf{P}_3}\right) \cos(\theta_i)], \end{aligned} \tag{9}$$

where $\theta_{\Delta\mathbf{P}_i}$ and $\varphi_{\Delta\mathbf{P}_i}$ are the elevation and azimuth of the distance vectors $\Delta\mathbf{P}_i$, $i = 1, 2, 3$ in the global coordinate system. The distance vector $\Delta\mathbf{P}_1$ is parallel to Z-axis, thus the elevation and azimuth of $\Delta\mathbf{P}_1$ are respectively expressed as

$$\theta_{\Delta\mathbf{P}_1} = 0, \varphi_{\Delta\mathbf{P}_1} = \pi/2. \tag{10}$$

The elevation and azimuth of $\Delta\mathbf{P}_2$ are respectively expressed as

$$\theta_{\Delta\mathbf{P}_2} = \pi/2, \varphi_{\Delta\mathbf{P}_2} = \pi/3. \tag{11}$$

The elevation and azimuth of $\Delta\mathbf{P}_3$ are respectively expressed as

$$\theta_{\Delta\mathbf{P}_3} = \pi/2, \varphi_{\Delta\mathbf{P}_1} = 2\pi/3 \tag{12}$$

The generalized steering vectors (GSVs) of $\mathbf{X}_1(t)$, $\mathbf{X}_2(t)$, $\mathbf{X}_3(t)$ and $\mathbf{X}_4(t)$ can be respectively expressed as

$$\mathbf{b}_1(\boldsymbol{\mu}_i) = \int\int \mathbf{a}(\theta,\varphi)\,\rho_i(\theta,\varphi;\boldsymbol{\mu}_i)\,d\theta d\varphi, \tag{13}$$

$$\mathbf{b}_2(\boldsymbol{\mu}_i) = \int\int \mathbf{a}(\theta,\varphi)\exp(-j\omega_{1i}) \times\rho_i(\theta,\varphi;\boldsymbol{\mu}_i)\,d\theta d\varphi, \tag{14}$$

$$\mathbf{b}_3(\boldsymbol{\mu}_i) = \int\int \mathbf{a}(\theta,\varphi)\exp(-j\omega_{2i}) \times\rho_i(\theta,\varphi;\boldsymbol{\mu}_i)\,d\theta d\varphi, \tag{15}$$

For $d_1/\lambda = 1/4$ and a small augular extension, there is an approximate rotational invariance relationship between $\mathbf{b}_1(\boldsymbol{\mu}_i)$ and $\mathbf{b}_2(\boldsymbol{\mu}_i)$ as follows (the proof is given in Appendix.)

$$\mathbf{b}_2(\boldsymbol{\mu}_i) \approx \mathbf{b}_1(\boldsymbol{\mu}_i)\exp(-jl\cos\theta_i), \tag{16}$$

where $l = 2\pi d_1/\lambda$. The matrix form can be written as

$$\mathbf{B}_2 \approx \mathbf{B}_1\boldsymbol{\Phi}_1, \tag{17}$$

where

$$\mathbf{B}_1 = \left[\mathbf{b}_1(\boldsymbol{\mu}_1), \mathbf{b}_1(\boldsymbol{\mu}_2), \ldots, \mathbf{b}_1(\boldsymbol{\mu}_D)\right], \tag{18}$$

$$\mathbf{B}_2 = \left[\mathbf{b}_2(\boldsymbol{\mu}_2), \mathbf{b}_1(\boldsymbol{\mu}_2), \ldots, \mathbf{b}_2(\boldsymbol{\mu}_D)\right], \tag{19}$$

$$\boldsymbol{\Phi}_1 = \mathrm{diag}\left[\exp(-jl\cos\theta_1), \ldots, \exp(-jl\cos\theta_D)\right]. \tag{20}$$

For $d_1/\lambda = 1/4$ and a small augular extension, the similar relationships hold as follows (the proof is given in Appendix.)

$$\mathbf{b}_3(\boldsymbol{\mu}_i) \approx \frac{H_3}{H_1}\exp(-j\omega_{2i})\,\mathbf{b}_1(\boldsymbol{\mu}_i), \tag{21}$$

$$\mathbf{b}_4(\boldsymbol{\mu}_i) \approx \frac{H_4}{H_1}\exp(-j\omega_{3i})\,\mathbf{b}_1(\boldsymbol{\mu}_i). \tag{22}$$

The matrix form can be respectively written as

$$\mathbf{B}_3 \approx \mathbf{B}_1\boldsymbol{\Phi}_2, \tag{23}$$

$$\mathbf{B}_4 \approx \mathbf{B}_1\boldsymbol{\Phi}_3, \tag{24}$$

where

$$\mathbf{B}_3 = \left[\mathbf{b}_3(\boldsymbol{\mu}_1), \mathbf{b}_3(\boldsymbol{\mu}_2), \ldots, \mathbf{b}_3(\boldsymbol{\mu}_D)\right], \tag{25}$$

$$\mathbf{B}_4 = \left[\mathbf{b}_4(\boldsymbol{\mu}_1), \mathbf{b}_4(\boldsymbol{\mu}_2), \ldots, \mathbf{b}_4(\boldsymbol{\mu}_D)\right], \tag{26}$$

$$\boldsymbol{\Phi}_2 = \mathrm{diag}\left[\frac{H_2}{H_1}\exp(-j\omega_{21}), \ldots, \frac{H_2}{H_1}\exp(-j\omega_{2D})\right] \tag{27}$$

$$\boldsymbol{\Phi}_3 = \mathrm{diag}\left[\frac{H_3}{H_1}\exp(-j\omega_{31}), \ldots, \frac{H_3}{H_1}\exp(-j\omega_{3D})\right] \tag{28}$$

By collecting N snapshot number, thus the received data matrices $\mathbf{X}_1, \mathbf{X}_2, \mathbf{X}_3$ and $\mathbf{X}_4$ can be respectively rewritten as

$$\mathbf{X}_1 = \mathbf{B}_1\mathbf{S} + \mathbf{N}_1, \tag{29}$$

$$\mathbf{X}_2 = \mathbf{B}_1\boldsymbol{\Phi}_1\mathbf{S} + \mathbf{N}_2, \tag{30}$$

$$\mathbf{X}_3 = \mathbf{B}_1\boldsymbol{\Phi}_2\mathbf{S} + \mathbf{N}_3, \tag{31}$$

$$\mathbf{X}_4 = \mathbf{B}_1\boldsymbol{\Phi}_3\mathbf{S} + \mathbf{N}_4. \tag{32}$$

The total received data vector of the sub-arrays can be constructed as

$$\mathbf{X} = \left[\mathbf{X}_1^T\ \mathbf{X}_2^T\ \mathbf{X}_3^T\ \mathbf{X}_4^T\right]^T. \tag{33}$$

3 2-D DOA estimation via PM

The manifold matrix $\mathbf{B}_1$ is full column rank, thus D rows of $\mathbf{B}_1$ are linear independent. Other rows can be linearly represented by these D rows. $\mathbf{B}_1$ can be partitioned into two blocks

$$\mathbf{B}_1 = \left[\mathbf{C}_1^T\ \mathbf{C}_2^T\right]^T, \tag{34}$$

where $\mathbf{C}_1$ is a $D \times D$ matrix; $\mathbf{C}_2$ is a $(m-D) \times D$ matrix. A propagator can be defined as the unique linear operator $\mathbf{P}$ from $(m-D)$-dimensional complex space $\mathbb{C}^{m-D}$ to D-dimensional complex space $\mathbb{C}^D$. The relationship between $\mathbf{C}_1$ and $\mathbf{C}_2$ is expressed as

$$\mathbf{P}^H\mathbf{C}_1 = \mathbf{C}_2. \tag{35}$$

Construct a new matrix $\mathbf{C}$ as follows

$$\mathbf{C} = \left[\mathbf{B}_1^T\ \left(\mathbf{B}_1^T\boldsymbol{\Psi}_1\right)^T\ \left(\mathbf{B}_1^T\boldsymbol{\Psi}_2\right)^T\ \left(\mathbf{B}_1^T\boldsymbol{\Psi}_3\right)^T\right]^T. \tag{36}$$

$\mathbf{C}$ can be partitioned into two blocks

$$\mathbf{C} = \left[\mathbf{C}_1^T\ \mathbf{D}_1^T\right]^T, \tag{37}$$

where

$$\mathbf{D}_1 = \left[\mathbf{C}_2^T\ (\mathbf{C}_1\Psi_1)^T\ (\mathbf{C}_2\Psi_1)^T\ (\mathbf{C}_1\Psi_2)^T\ (\mathbf{C}_2\Psi_2)^T\ (\mathbf{C}_1\Psi_3)^T\ (\mathbf{C}_2\Psi_3)^T\right]^T \tag{38}$$

According to Eq. 36, the matrix $\mathbf{C}_1$ and $\mathbf{D}_1$ satisfies $\mathbf{D}_1 = \bar{\mathbf{V}}^H\mathbf{C}_1$, where $\bar{\mathbf{V}}$ is a $D \times (4m-D)$ matrix. Partition (34) into two block matrices, we have

$$\mathbf{X} = \left[\mathbf{X}_1^T\ \mathbf{X}_2^T\right]^T, \tag{39}$$

where $\mathbf{X}_1$ is a $D \times N$ matrix; X_2 is a $(4m-D) \times N$ matrix. The relationship between $\mathbf{X}_1$ and $\mathbf{X}_2$ is expressed as

$$\mathbf{X}_2 = \bar{\mathbf{V}}^H\mathbf{X}_1. \tag{40}$$

In practical application, the left side of Eq. 41 does not really equal to the right side of Eq. 41. Thus a least square solution is given by

$$\overline{\mathbf{V}} = \left(\mathbf{X}_1\mathbf{X}_1^H\right)^{-1}\mathbf{X}_1\mathbf{X}_2^H. \tag{41}$$

We divide $\overline{\mathbf{V}}$ into seven block matrices $\overline{\mathbf{V}}_1 - \overline{\mathbf{V}}_7$, which correspond to the dimensions of seven matrices of $\mathbf{D}_1$. According to Eq. 39, we have

$$\overline{\mathbf{V}_1}^{\#}\overline{\mathbf{V}_3}\mathbf{C}_1 = \mathbf{C}_1\mathbf{\Psi}_1, \tag{42}$$

$$\overline{\mathbf{V}_1}^{\#}\overline{\mathbf{V}_5}\mathbf{C}_1 = \mathbf{C}_1\mathbf{\Psi}_2, \tag{43}$$

$$\overline{\mathbf{V}_1}^{\#}\overline{\mathbf{V}_7}\mathbf{C}_1 = \mathbf{C}_1\mathbf{\Psi}_3. \tag{44}$$

The eigendecompostion of the matrices $\overline{\mathbf{V}_1}^{\#}\overline{\mathbf{V}_3}$, $\overline{\mathbf{V}_1}^{\#}\overline{\mathbf{V}_5}$ and $\overline{\mathbf{V}_1}^{\#}\overline{\mathbf{V}_7}$ yields their eigenvalues λ_{1i}, λ_{2i} and λ_{3i} and the corresponding eigenvector $\mathbf{u}_{1i}$, $\mathbf{u}_{2i}$ and $\mathbf{u}_{3i}$, respectively, $i = 1, 2, \cdots, M$. Arrange their eigenvalues in descending sequence we have $\lambda_{11} \geq \cdots \geq \lambda_{1D}$, $\lambda_{21} \geq \cdots \geq \lambda_{2D}$ and $\lambda_{31} \geq \cdots \geq \lambda_{3D}$, respectively. Three diagonal matrices are constructed as $\tilde{\mathbf{\Psi}}_1 = \text{diag}\{\lambda_{11}, \cdots, \lambda_{1D}\}$, $\tilde{\mathbf{\Psi}}_2 = \text{diag}\{\lambda_{21}, \cdots, \lambda_{2D}\}$ and $\tilde{\mathbf{\Psi}}_3 = \text{diag}\{\lambda_{31}, \cdots, \lambda_{3D}\}$ whose elements include the nominal DOAs of CD sources corresponding to $\mathbf{\Psi}_1$, $\mathbf{\Psi}_2$ and $\mathbf{\Psi}_3$, respectively. Thus the nominal elevation and azimuth DOAs of CD sources can be achieved.

However, the eigendecompostions of $\overline{\mathbf{V}_1}^{\#}\overline{\mathbf{V}_3}$, $\overline{\mathbf{V}_1}^{\#}\overline{\mathbf{V}_5}$ and $\overline{\mathbf{V}_1}^{\#}\overline{\mathbf{V}_7}$ are individually taken. When $D \geq 2$, this may result in the problem of the mismatching of the eigenvalues, i.e, the nominal elevation DOAs and the nominal azimuth DOAs cannot be paired effectively. To deal with this problem, we have the following method. First, the eigendecomposion of the matrix $\overline{\mathbf{V}_1}^{\#}\overline{\mathbf{V}_3}$, is taken, and the eigenvalues λ_{1i} and the corresponding eigenvectors $\mathbf{u}_{1i}$ are obtained. According to Eqs. 44 and 45, we know that $\overline{\mathbf{V}_1}^{\#}\overline{\mathbf{V}_5}$ and $\overline{\mathbf{V}_1}^{\#}\overline{\mathbf{V}_7}$ have the same eigenvectors as $\overline{\mathbf{V}_1}^{\#}\overline{\mathbf{V}_3}$, thus $\mathbf{u}_{1i}$ are the eigenvectors of $\overline{\mathbf{V}_1}^{\#}\overline{\mathbf{V}_5}$ and $\overline{\mathbf{V}_1}^{\#}\overline{\mathbf{V}_7}$. According to the definition of the eigenvectors and eigenvalues of the matrix, we have

$$\overline{\mathbf{V}_1}^{\#}\overline{\mathbf{V}_5}\cdot\mathbf{u}_{1i} = \lambda_{2i}\cdot\mathbf{u}_{1i}, \tag{45}$$

$$\overline{\mathbf{V}_1}^{\#}\overline{\mathbf{V}_7}\cdot\mathbf{u}_{1i} = \lambda_{3i}\cdot\mathbf{u}_{1i}, \tag{46}$$

where

$$\mathbf{u}_{1i} = [\eta_{i1}, \cdots, \eta_{iD}]^{\mathrm{T}}, \tag{47}$$

$$\overline{\mathbf{V}_1}^{\#}\overline{\mathbf{V}_5}\cdot\mathbf{u}_{1i} = [p_{i1}, \cdots, p_{iD}]^{\mathrm{T}}, \tag{48}$$

$$\overline{\mathbf{V}_1}^{\#}\overline{\mathbf{V}_7}\cdot\mathbf{u}_{1i} = [q_{i1}, \cdots, q_{iD}]^{\mathrm{T}}. \tag{49}$$

Based on Eq. 46–50, $\mathbf{u}_{2i}$ and $\mathbf{u}_{3i}$ can be respectively rewritten as

$$\lambda_{2i} = \frac{1}{D}\sum_{j=1}^{D}\frac{p_{ij}}{u_{ij}}, (i = 1, 2, \cdots, D), \tag{50}$$

$$\lambda_{3i} = \frac{1}{D}\sum_{j=1}^{D}\frac{q_{ij}}{u_{ij}}, (i = 1, 2, \cdots, D). \tag{51}$$

Since H_1, H_2 and H_3 are real numbers, the phase ambiguity caused by the positive and negative inconsistency of H_1, H_2 and H_3 can be eliminated by squaring λ_{2i} and λ_{3i}. Then Eqs. 7, 8 and 9 can be expressed as

$$\omega_{1i} = -\text{angle}\left(\lambda_{1i}\right), \tag{52}$$

$$\begin{aligned}\omega_{2i} &= -\frac{1}{2}\text{angle}\left(\left[\frac{H_3}{H_1}\exp\left(-j\omega_{2i}\right)\right]^2\right)\\ &= -\frac{1}{2}\text{angle}\left(\exp\left(-j\omega_{2i}\right)^2\right) = -\frac{1}{2}\text{angle}\left(\left(\lambda_{2i}\right)^2\right),\end{aligned} \tag{53}$$

$$\omega_{3i} = -\frac{1}{2}\text{angle}\left(\left(\lambda_{3i}\right)^2\right). \tag{54}$$

Assume $\Delta p_{i1} = \sin\left(\theta_{\Delta\mathbf{P}_i}\right)\cos\left(\varphi_{\Delta\mathbf{P}_i}\right)$, $\Delta p_{i2} = \sin\left(\theta_{\Delta\mathbf{P}_i}\right)\sin\left(\varphi_{\Delta\mathbf{P}_i}\right)$ and $\Delta p_{i3} = \cos\left(\theta_{\Delta\mathbf{P}_i}\right)$, $(i = 1, 2, 3)$. We can write Eqs. 53–55 in matrix form as

$$-\frac{\lambda}{2\pi}\begin{bmatrix}\frac{angle(\lambda_{1i})}{d_1}\\ \frac{angle((\lambda_{2i})^2)}{2d_2}\\ \frac{angle((\lambda_{3i})^2)}{2d_3}\end{bmatrix} = \begin{bmatrix}\Delta p_{11} & \Delta p_{12} & \Delta p_{13}\\ \Delta p_{21} & \Delta p_{22} & \Delta p_{23}\\ \Delta p_{31} & \Delta p_{32} & \Delta p_{33}\end{bmatrix}\begin{bmatrix}\gamma_{1i}\\ \gamma_{2i}\\ \gamma_{3i}\end{bmatrix}. \tag{55}$$

Then the solution of Eq. 56 is given by

$$\begin{bmatrix}\gamma_{1i}\\ \gamma_{2i}\\ \gamma_{3i}\end{bmatrix} = -\frac{\lambda}{2\pi}\begin{bmatrix}\Delta p_{11} & \Delta p_{12} & \Delta p_{13}\\ \Delta p_{21} & \Delta p_{22} & \Delta p_{23}\\ \Delta p_{31} & \Delta p_{32} & \Delta p_{33}\end{bmatrix}^{-1}\begin{bmatrix}\frac{angle(\lambda_{1i})}{d_1}\\ \frac{angle((\lambda_{2i})^2)}{2d_2}\\ \frac{angle((\lambda_{3i})^2)}{2d_3}\end{bmatrix}. \tag{56}$$

The information about the nominal elevation and azimuth DOAs of CD sources is contained in γ_{1i}, γ_{2i} and γ_{3i}. The DOAs of CD sources can be obtained after simple trigonometric function operator. Then we can summarize the proposed generalized steering vectors-propagator method (GSVPM) in **Algorithm 1**.

Algorithm 1 GSVPM

1: Construct the total received data vector of the sub-arrays $\mathbf{X}$ according to (34);
2: Estimate propagator $\overline{\mathbf{V}}$ according to (42);
3: Partition $\overline{\mathbf{V}}$ into seven sub-matrices according to (39);
4: Estimate $\mathbf{\Psi}_1$, $\mathbf{\Psi}_2$ and $\mathbf{\Psi}_3$ according to (43)–(45);
5: Complete the parameter pairing according to (46) and (47);
6: Estimate the nominal azimuth and elevation DOAs of CD sources from the corresponding eigenvalues (51) and (52) by calculating (57).

By exploiting the rotational invariance property of the arrays structure, the proposed algorithm can be applied to other arrays with different configuration such conical arrays and sphere arrays. In general, two different rotational invariance matrices are constructed, and then the azimuth and elevation estimation can be achieved by the proposed algorithms with little modification.

4 Distributed and parallel processing

In real application such as passive bistatic radar systems, the common observed time is 1s [28]. Assume the sampling frequency of analog to digital converter (ADC) is 400 MHz. The number of sampling points in each channel is 400×10^6. For array 1, the number of elements is $3m + 1 = 28$ with $m = 9$. The total number of elements of the whole array is $3 \times 28 = 84$. The sampling points of the whole received data is 3.36×10^{10}, which means the amount of data is tremendous. In order to improve the computing speed, we divide the sampling points of 28 elements into several fractions as shown in Fig. 3.

For array 1, L fractions can be processed in parallel based on the proposed algorithm with the help of multi-core processor (MCP). Since the importance of L fractions is identical, the weights of L fractions equal to each other. Thus we just need to average the parameter values (the nominal azimuth and elevation DOAs of CD sources) when L computing results return.

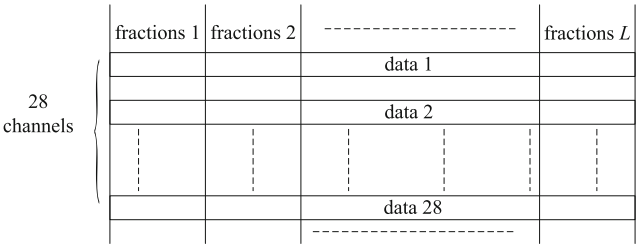

Fig. 3 The fractional division of the received data of array 1

Since we use three arrays to cover the whole space, each array is equipped with one MCP. Three arrays work in a distributed way. The estimation results of three arrays would return to the data processing center (DPC) as shown in Fig. 4. The signal may come from any directions of the whole space. If the signal strength that one array receives is much larger than other two arrays. The estimation result with high signal strength would be regarded as the real DOAs of the incident CD sources.

5 Computational complexity analysis

In previous Section, we discuss the computing way for DOA estimation of CD sources with big data. The distributed and parallel method are adopted to deal with this problem. However, if the computational complexity of algorithm is high, this would result in large energy consumption. In this Section, we will compare the computational complexity of the proposed algorithm with SOS [15], QRIP [16] and ESPRIT-based [26] algorithms. For the sake of simplicity, we only focus on the computational complexity of the complex multiplication. The 1-D searching is needed for SOS algorithm, the computational complexity of SOS focuses on the construction of the $2m \times 2m$ sampling covariance matrix and its eigendecomposition. This would cost $O\left(4m^2N\right) + O\left(8m^3\right) + O\left(2m^6\right)$, where m is the number of elements in the same generatrix, and N is the snapshot number. For the QRIP algorithm, the computational complexity focuses on the construction of the $m \times m$ and the $2m \times 2m$ sampling covariance matrix and their eigendecomposition. This would cost $O\left(5m^2N\right) + O\left(9m^3\right)$. For the ESPRIT-based algorithm, the computational complexity focus on the eigendecomposition of three $2m \times 2m$ sampling covariance matrix, this would cost $O\left(12m^2N\right) + O\left(24m^3\right)$. The computational complexity of the proposed algorithm focuses on estimating propagator and eigendecomposition of three $D \times D$ matrices, where D is the source number.

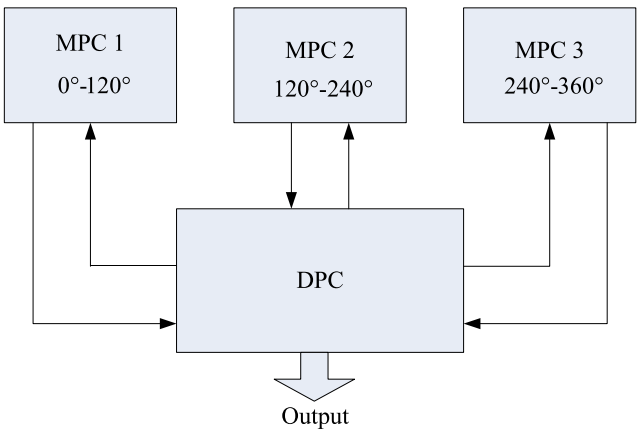

Fig. 4 The distributed computing based on three MPCs

This would cost $O\left(4D^3\right)+O\left(3ND^2\right)+O\left(4mDN\right)$. Generally, $N \gg m > D$, thus the computational complexity of the proposed algorithm is the lowest of all the algorithms mentioned above.

6 Simulation results

In order to verify the effectiveness of the proposed algorithm, i.e., GSVPM, the estimation performance of the proposed algorithm is compared with SOS [15] and ESPRIT-based [26] algorithms. Each simulated point is obtained as an average of 400 independent Monte Carlo simulation trials. The array geometry is depicted in Fig. 1a. The number of the elements in array 1 is 25, i.e., the number of elements in the same generatrix is $m = 8$. The polarization parameter are $k_{1\theta} = 0.5$, $k_{1\varphi} = 0.5$, $k_{2\theta} = 0.3$, $k_{2\varphi} = 0.7$. The expression of elements pattern are $g_{i\theta}=\sin\left(\theta'_j-\varphi'_j\right)$, $g_{i\varphi}=\cos\left(\theta'_j-\varphi'_j\right)$, where θ'_j and φ'_j are the azimuth and elevation of the jth signal corresponding to ith element in local coordinate system. For SOS and ESPRIT-based algorithms, the elements $1 \sim m$ and $2 \sim m+1$ construct the first sub-array pairing; the elements $m+3 \sim 2m+2$ and $2m+4 \sim 3m+3$ construct the second sub-array pairing. A successful trial is defined as the trial whose estimation bias is less than 1°. The successful probability is defined as the ratio between the number of successful trials and total trials. The root-mean-square-error (RMSE) is defined as

$$RMSE=\sqrt{\frac{1}{M}\sum_{t=1}^{M}\left[\left(\hat{\theta}_{it}-\theta\right)^2+\left(\hat{\varphi}_{it}-\varphi\right)^2\right]}, \tag{57}$$

where $\hat{\theta}_{it}$ and $\hat{\varphi}_{it}$ respectively stand for the estimation values of azimuth and elevation of the ith signal in the tth trials; θ and φ stand for the real values of azimuth and elevation, respectively.

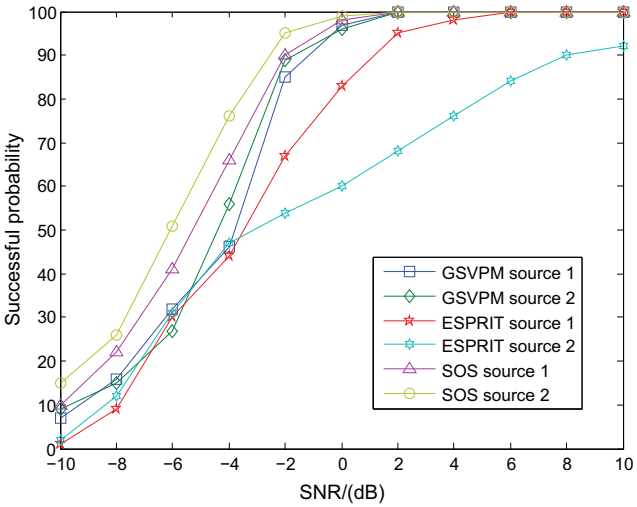

Fig. 6 The successful probability versus SNR

In the first example, the Gaussian shaped CD sources with parameter vector $\boldsymbol{\mu}_1 = (100°, 3°, 60°, 4°)$ and $\boldsymbol{\mu}_2 = (95°, 2°, 50°, 2°)$ are adopted. The RMSE and successful probability of different algorithms versus SNR are depicted in Figs. 5 and 6, respectively. The snapshot number is fixed at 400. It can be seen from Fig. 5 that the RMSE of GSVPM is smaller than that of ESPRIT-based algorithm. The GSVPM would approach the SOS algorithm with SNR increases. This mainly caused by that the GSVPM adopts three sub-array pairings to estimate DOAs of CD sources. However, the ESPRIT adopts two sub-array pairings. The data used by GSVPM is larger than that of ESPRIT algorithm. The SOS adopts spectrum peaking searching to guarantee the high estimation accuracy.

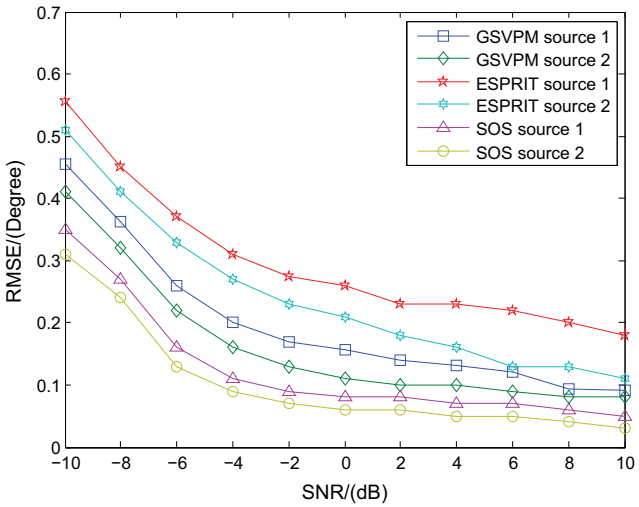

Fig. 5 The RMSE versus SNR

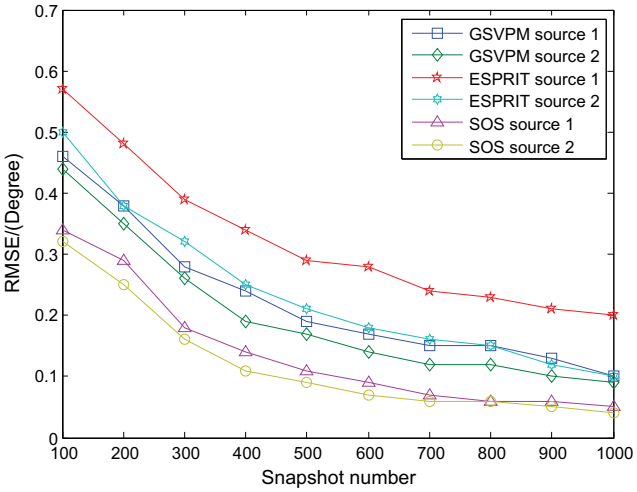

Fig. 7 The RMSE versus SNR

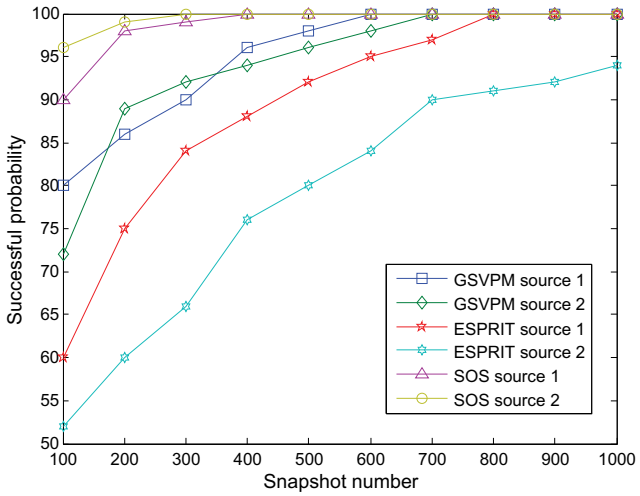

Fig. 8 The successful probability versus SNR

It can be seen from Fig. 6 that the successful probability of GSVPM and ESPRIT are similar at low SNR. However, the successful probability of GSVPM is higher than that of ESPRIT algorithm at high SNR. When SNR reaches 2dB, the successful probability of GSVPM and SOS both approach 100 %. However, the successful probability of ESPRIT algorithm is lower than that of the algorithm mentioned above. More data has been used in GSVPM, thus it has high successful probability.

In the second example, the RMSE and successful probability of different algorithms versus snapshot number are depicted in Figs. 7 and 8, respectively. The signal source parameters are identical with the first example. The SNR is fixed at 0dB. It can be seen from Fig. 7 that the RMSE of different algorithms decreases with snapshot number increases. The RMSE of GSVPM is smaller than that of ESPRIT algorithm. The GSVPM would approach the SOS algorithm with snapshot number increases. Our algorithm present accurate estimation even for a small snapshot number, since more data has been used.

It can be seen from Fig. 8 that the successful probability of SOS would reach 100 % when snapshot number reaches 400. However, the GSVPM needs 700 snapshot number. The successful probability of GSVPM is higher than that of ESPRIT algorithm at small snapshot number. The reason is that the GSVPM adopts more data than that of ESPRIT algorithm.

7 Conclusion

In this paper, in order to enhance the transmission performance of D2D communication in massive MIMO system, a low computational complexity 2-D DOA estimation algorithm of CD sources is proposed based on conformal array. Based on GSVs, the proposed algorithm construct three rational invariance relationships. Then the PM is used for DOA estimation. Without spectrum peaking searching, and estimation and eigendecomposition of sampling covariance matrix, the proposed algorithm has low computational complexity. Since the amount of data is tremendous, the distributed and parallel scheme has been proposed to accelerate the computing of the proposed algorithm. Thus the estimation accuracy of CD sources can be guaranteed in a related short time. In the future, we will focus on 2-D DOA estimation for ID sources with low computational complexity.

Acknowledgments The work is supported by "Qing Lan Project" and "the National Natural Science Foundation of China under Grant No.61572172 and No.61602152" and supported by "the Fundamental Research Funds for the Central Universities, No.2016B10714 and No.2016B03114" and supported by "Science & Technology Pillar Program (Social development) of Changzhou Science and Technology Bureau, No.CE20165023".

Appendix: The derivation of Eq. 18

Assume that the coordinate of each element is (x_k, y_k, z_k), $k = 1, 2, \cdots, m$. The unit vectors of X-axis, Y-axis and Z-axis are given by $\vec{\mathbf{e}}_x$, $\vec{\mathbf{e}}_y$ and $\vec{\mathbf{e}}_z$, respectively. The position vector $\mathbf{p}_k$ of kth element is expressed as

$$\mathbf{p}_k = x_k \vec{\mathbf{e}}_x + y_k \vec{\mathbf{e}}_y + z_k \vec{\mathbf{e}}_z, \tag{58}$$

For sub-array 1 and sub-array 2, the elements are arranged on the same generatrix, the X-axis and Y-axis coordinates of the elements in the same generatrix have the relationship $x_{11} = \cdots = x_{1(m+1)} = x_1$ and $y_{11} = \cdots = y_{1(m+1)} = y_1$, respectively. The patterns of the elements in the same generatrix are identical as well, i.e., $h_{11} = \cdots = h_{1(m+1)}$. The kth element of the steering vector $\mathbf{b}_1(\boldsymbol{\mu}_i)$ of sub-array 1 can be expressed as

$$\begin{aligned}\left[\mathbf{b}_1(\boldsymbol{\mu}_i)\right]_k &= \int\int a_{1k}(\theta,\varphi)\,\rho(\theta,\varphi;\boldsymbol{\mu}_i)\,d\theta d\varphi \\ &= H_1 \int\int \exp\left[-jl(k-1)\cos\theta\right]\rho(\theta,\varphi;\boldsymbol{\mu}_i)\,d\theta d\varphi,\end{aligned} \tag{59}$$

where the kth element of the steering vector of sub-array 1 is $a_{1k}(\theta,\varphi) = H_1 \exp\left[-jl(k-1)\cos\theta\right]$ with

$$H_1 = h_1 \exp\left(-j2\pi \frac{x_1 \sin\theta\cos\varphi + y_1 \sin\theta \sin\varphi}{\lambda}\right). \tag{60}$$

The azimuth and elevation DOAs can be expressed as

$$\theta = \theta_i + \tilde{\theta}, \tag{61}$$

$$\varphi = \varphi_i + \tilde{\varphi}, \tag{62}$$

where θ_i and φ_i are nominal elevation and azimuth of ith CD source, and they are the means of θ and φ, respectively; $\tilde{\theta}$ and $\tilde{\varphi}$ are the corresponding random angular deviations. With the first order Taylor series approximation to $a_{1k}(\theta, \varphi)$ around $(\theta, \varphi) = (\theta_i, \varphi_i)$, we can obtain

$$\begin{aligned} & a_{1k}(\theta, \varphi) = H_1 \exp\left[-jl(k-1)\cos\theta\right] \\ & = H_1 \exp\left[-jl(k-1)\cos\left(\theta_i + \tilde{\theta}\right)\right] \\ & = H_1 \exp\left[-jl(k-1)\left[\cos\theta_i\cos\tilde{\theta} - \sin\theta_i \sin\tilde{\theta}\right]\right] \\ & \approx H_1 \exp\left[-jl(k-1)\left(\cos\theta_i - \tilde{\theta}\sin\theta_i\right)\right], \end{aligned} \tag{63}$$

where $\cos\tilde{\theta} \approx 1$ and $\sin\tilde{\theta} \approx \tilde{\theta}$ are used in the first inequality for a small angular extension. Then Eq. 59 can be written as

$$\begin{aligned} \left[\mathbf{b}_1(\boldsymbol{\mu}_i)\right]_k &= \int\int a_{1k}(\theta, \varphi)\, \rho\left(\theta, \varphi; \boldsymbol{\mu}_i\right) d\theta d\varphi \\ &\approx H_1 \exp\left[-jl(k-1)\cos\theta_i\right]\left[h\left(\boldsymbol{\mu}_i\right)\right]_k, \end{aligned} \tag{64}$$

where

$$\begin{aligned} \left[h\left(\boldsymbol{\mu}_i\right)\right]_k = \int\int & \exp\left[jl(k-1)\tilde{\theta}\sin\theta\right] \\ & \times \rho_i\left(\theta_i + \tilde{\theta}, \varphi_i + \tilde{\varphi}; \boldsymbol{\mu}_i\right) d\tilde{\theta} d\tilde{\varphi}, \end{aligned} \tag{65}$$

The kth element of the steering vector $\mathbf{b}_2\left(\boldsymbol{\mu}_i\right)$ of sub-array 2 can be expressed as

$$\begin{aligned} \left[\mathbf{b}_2\left(\boldsymbol{\mu}_i\right)\right]_k = & \int\int a_{2k}(\theta, \varphi) \exp(-jlcos\theta) \\ & \times \rho_i\left(\theta_i + \tilde{\theta}, \varphi_i + \tilde{\varphi}; \mu_i\right) d\tilde{\theta} d\tilde{\varphi} \\ \approx & H_1 \exp\left[-jl(k-1)\cos\theta_i\right] \\ & \int\int \exp\left[jl(k-1)\tilde{\theta}\sin\theta_i\right] \\ & \times \exp(-jlcos\theta_i) \exp\left(jl\tilde{\theta}\sin\theta_i\right) \\ & \times \rho_i\left(\theta_i + \tilde{\theta}, \varphi_i + \tilde{\varphi}; \boldsymbol{\mu}_i\right) d\tilde{\theta} d\tilde{\varphi}. \end{aligned} \tag{66}$$

For a small angular extension and $d_1/\lambda = 1/4$, it follows that $\exp\left(jl\tilde{\theta}\sin\theta_i\right) \approx 1$. Then $\mathbf{b}_2\left(\boldsymbol{\mu}_i\right)$ can be expressed as

$$\begin{aligned} \left[\mathbf{b}_2\left(\boldsymbol{\mu}_i\right)\right]_k \approx & H_1 \exp\left[-jl(k-1)\cos\theta_i\right] \\ & \times \exp(-jlcos\theta_i)\left[h\left(\boldsymbol{\mu}_i\right)\right]_k. \end{aligned} \tag{67}$$

Based on Eqs. 64 and 67, an approximate rotational invariance relationship between $\mathbf{b}_1\left(\boldsymbol{\mu}_i\right)$ and $\mathbf{b}_2\left(\boldsymbol{\mu}_i\right)$ can be given by

$$\mathbf{b}_2\left(\boldsymbol{\mu}_i\right) \approx \exp(-jlcos\theta_i)\, \mathbf{b}_1\left(\boldsymbol{\mu}_i\right). \tag{68}$$

The derivation of Eqs. 24 and 25

For sub-array 3, the X-axis and Y-axis coordinates of the elements in the same generatrix have the relationship $x_{3(m+3)} = x_{3(m+4)} \cdots = x_{3(2m+2)} = x_3$ and $y_{3(m+3)} = y_{3(m+4)} \cdots = y_{3(2m+2)} = y_3$, respectively. The patterns of the elements in the same generatrix are identical as well, i.e., $h_{3(m+3)} = h_{3(m+4)} \cdots = h_{3(2m+2)}$. The kth element of the steering vector $\mathbf{b}_3\left(\boldsymbol{\mu}_i\right)$ of sub-array 3 can be expressed as

$$\begin{aligned} \left[b_3\left(\boldsymbol{\mu}_i\right)\right]_k = & \int\int a_{3k}(\theta, \varphi)\, \rho\left(\theta, \varphi; \boldsymbol{\mu}_i\right) d\theta d\varphi \\ = & H_3 \int\int \exp\left[-jl(k-1)\cos\theta\right] \\ & \times \exp(-j\omega_2)\, \rho\left(\theta, \varphi; \boldsymbol{\mu}_i\right) d\theta d\varphi \\ = & H_3 \int\int \exp\left[-jl(k-1)\cos\theta\right] \\ & \times \exp\left[-jl\left(\frac{1}{2}\sin\theta\cos\varphi + \frac{\sqrt{3}}{2}\sin\theta\sin\varphi\right)\right] \\ & \times \rho\left(\theta, \varphi; \boldsymbol{\mu}_i\right) d\theta d\varphi, \end{aligned} \tag{69}$$

where $\exp(-j\omega_{2i}) = \exp[-jl(\frac{1}{2}\sin\theta\cos\varphi + \frac{\sqrt{3}}{2}\sin\theta\sin\varphi)]$ according to Eqs. 8 and 11; the kth element of the steering vector of sub-array 1 is $a_{3k}(\theta, \varphi) = H_3 \exp\left[-jl(k-1)\cos\theta\right]$ with

$$H_3 = h_3 \exp\left(-j2\pi\frac{x_3\sin\theta\cos\varphi + y_3\sin\theta\sin\varphi}{\lambda}\right). \tag{70}$$

With the first order Taylor series approximation to $\exp\left(-\frac{1}{2}jl\sin\theta\cos\varphi\right)$ and $\exp\left(-\frac{\sqrt{3}}{2}jl\sin\theta\sin\varphi\right)$, we respectively have

$$\begin{aligned} & \exp\left(-\frac{1}{2}jl\sin\theta\cos\varphi\right) \\ & = \exp\left[-\frac{1}{2}jl\sin\left(\theta_i + \tilde{\theta}\right)\cos\left(\varphi_i + \tilde{\varphi}\right)\right] \\ & \approx \exp\left[-\frac{1}{2}jl\left(\sin\theta_i + \tilde{\theta}\cos\theta_i\right)\left(\cos\varphi_i + \tilde{\varphi}\sin\varphi_i\right)\right] \\ & \approx \exp\left(-\frac{1}{2}jl\sin\theta_i\cos\varphi_i\right) \\ & \quad \times \exp\left[-\frac{1}{2}jl\left(\tilde{\theta}\cos\theta_i\cos\varphi_i - \tilde{\varphi}\sin\varphi_i\sin\theta_i\right)\right] \end{aligned} \tag{71}$$

and

$$\begin{aligned}
&\exp\left(-\frac{\sqrt{3}}{2}jl\sin\theta\sin\varphi\right)\\
&=\exp\left[-\frac{\sqrt{3}}{2}jl\sin\left(\theta_i+\tilde{\theta}\right)\sin\left(\varphi_i+\tilde{\varphi}\right)\right]\\
&\approx\exp\left[-\frac{\sqrt{3}}{2}jl\left(\sin\theta_i+\tilde{\theta}\cos\theta_i\right)\left(\sin\varphi_i+\tilde{\varphi}\cos\varphi_i\right)\right]\\
&\approx\exp\left(-\frac{\sqrt{3}}{2}jl\sin\theta_i\sin\varphi_i\right)\\
&\quad\times\exp\left[-\frac{\sqrt{3}}{2}jl\left(\tilde{\theta}\cos\theta_i\sin\varphi_i+\tilde{\varphi}\cos\varphi_i\sin\theta_i\right)\right]
\end{aligned}\tag{72}$$

For a small angular extension and $d_2/\lambda = 1/4$, it follows that $\exp\left[-\frac{1}{2}jl\left(\tilde{\theta}\cos\theta_i\cos\varphi_i-\tilde{\varphi}\sin\varphi_i\sin\theta_i\right)\right]\approx 1$ and $\exp\left[-\frac{\sqrt{3}}{2}jl\left(\tilde{\theta}\cos\theta_i\sin\varphi_i+\tilde{\varphi}\cos\varphi_i\sin\theta_i\right)\right]\approx 1$. The kth element of the steering vector $\mathbf{b}_3\left(\boldsymbol{\mu}_i\right)$ of sub-array 3 can be expressed as

$$\begin{aligned}
&\left[\mathbf{b}_3\left(\boldsymbol{\mu}_i\right)\right]_k=\int\int a_{3k}\left(\theta,\varphi\right)\rho\left(\theta,\varphi;\boldsymbol{\mu}_i\right)d\theta d\varphi\\
&\approx H_1\exp\left[-jl\left(k-1\right)\cos\theta_i\right]\\
&\quad\times\exp\left[-jl\left(\frac{1}{2}\sin\theta_i\cos\varphi_i-\frac{\sqrt{3}}{2}\sin\theta_i\sin\varphi_i\right)\right]\\
&\quad\times\int\int\exp\left[jl\left(k-1\right)\tilde{\theta}\sin\theta_i\right]\rho\left(\theta,\varphi;\boldsymbol{\mu}_i\right)d\theta d\varphi\\
&\approx H_3\exp\left[-jl\left(k-1\right)\cos\theta_i\right]\exp\left(-j\omega_{2i}\right)\left[h\left(\boldsymbol{\mu}_i\right)\right]_k.
\end{aligned}\tag{73}$$

Based on Eqs. 59 and 73, an approximate rotational invariance relationship between $\mathbf{b}_1\left(\boldsymbol{\mu}_i\right)$ and $\mathbf{b}_3\left(\boldsymbol{\mu}_i\right)$ can be given by

$$\mathbf{b}_3\left(\boldsymbol{\mu}_i\right)\approx\frac{H_3}{H_1}\exp\left(-j\omega_{2i}\right)\mathbf{b}_1\left(\boldsymbol{\mu}_i\right).\tag{74}$$

Similar as Eq. 74, an approximate rotational invariance relationship between $\mathbf{b}_1\left(\boldsymbol{\mu}_i\right)$ and $\mathbf{b}_4\left(\boldsymbol{\mu}_i\right)$ can be given by

$$\mathbf{b}_4\left(\boldsymbol{\mu}_i\right)\approx\frac{H_4}{H_1}\exp\left(-j\omega_{3i}\right)\mathbf{b}_1\left(\boldsymbol{\mu}_i\right),\tag{75}$$

where the form of H_4 is similar with that of H_3.

References

1. Han G, Jiang J, Zhang C, Duong TQ, Guizani M, Karagiannidis G (2016) A Survey on mobile anchors assisted localization in wireless sensor networks. IEEE Commun Surveys Tuts doi:10.1109/COMST.2016.2544751
2. Mach P, Becvar Z, Vanek Z (2015) In-band device-to-device communication in OFDMA cellular networks: a survey and challenges. IEEE Commun Surveys Tuts 17(4):1885–1922
3. Han G, Liu L, Jiang J, Shu L, Hancke G (2015) Analysis of energy-efficient connected target coverage algorithms for industrial wireless sensor networks. IEEE Trans Ind Informat doi:10.1109/TII.2015.2513767
4. Asadi A, Wang Q, Mancuso V (2014) A survey on device-to-device communication in cellular networks. IEEE Commun Surveys Tuts 16(4):1801–1819
5. Ni Y, Jin S, Xu W, Matthaiou M, Shao S, Zhu H (2015) Beamforming and interference cancellation schemes for D2D communications. In: IEEE international conference on communication workshop (ICCW), pp 608–613
6. Marzetta TL (2010) Noncooperative cellular wireless with unlimited numbers of base station antennas. IEEE Trans Wireless Commun 9(11):3590–3600
7. Xu W, Liang L, Zhang H, Jin S, Li JCF, Lei M (2012) Performance enhanced transmission in device-to-device communications: beamforming or interference cancellation? In: IEEE Global communications conference (GLOBECOM), pp 4296–4301
8. Wan L, Han G, Jiang J, Rodrigues JJPC, Feng N, Zhu T (2015) DOA estimation for coherently distributed sources considering circular and noncircular signals in massive MIMO systems. IEEE Syst J doi:10.1109/JSYST.2015.2445052
9. Hu A, Lv T, Gao H, Zhang Z, Yang S (2014) An ESPRIT-based approach for 2D localization of incoherently distributed sources in massive MIMO systems. IEEE J Sel Top Signal Process 8(5):996–1011
10. Lv T, Tan F, Gao H, Yang S (2016) An ESPRIT-based approach for 2D localization of incoherently distributed sources in massive MIMO systems. Signal Process 121(C):30–45
11. Han G, Wan L, Shu L, Feng N (2015) Two novel DoA estimation approaches for real time assistant calibration system in future vehicle industrial. IEEE Syst J doi:10.1109/JSYST.2015.2434822
12. Wang TD, Gan L, Wei P, Liao HS (2013) DOA estimation of coherently distributed sources based on block-sparse constraint with measurement matrix uncertainty. IEICE Electronics Express 10(6):1–8
13. Zhou L, Li G, Zheng Z, Yang X (2014) Parameter estimation of coherently distributed sources using sparse representation. In: Proceedings of IEEE China summit & international conference on signal and information processing (ChinaSIP), pp 577–581
14. Han G, Dong Y, Guo H, Shu L, Wu D (2014) Cross-layer optimized routing in wireless sensor networks with duty-cycle and energy harvesting. Wirel Commun Mob Comput 15(16):1957–1981
15. Lee J, Song I, Kwon H, Lee SR (2003) Low-complexity estimation of 2D DOA for coherently distributed sources. Signal Process 83(8):1789–1802
16. Guo X, Wan Q, Yang W, Lei X (2009) Low-complexity 2D coherently distributed sources decoupled DOAs estimation method. Science in China Series F: Information Sciences 52(5):835–842
17. Zheng Z, Li G, Teng Y (2012) 2D DOA estimator for multiple coherently distributed sources using modified propagator. Circuits Syst Signal Process 31(1):255-270
18. Zheng Z, Li G, Teng Y (2012) Simplified estimation of 2D DOA for coherently distributed sources. Wireless Pers Commun 62(4):907–922
19. Zhang G, Tang B (2008) Decoupled estimation of 2D DOA for coherently distributed sources using 3D matrix pencil method. EURASIP Journal on Advances in Signal Processing Article No 151
20. Feng N, Yue Y, Zhu C, Wan L, Liu QH (2015) Second-order PML: optimal choice of nth-order PML for truncating FDTD domains. J Comput Phys 285:71–83

21. Popa BI, Allen J, Cummer SA (2009) Conformal array design with transformation electromagnetics. J Comput Phys 94:244102
22. Liu L, Jiang Y, Wan L, Tian Z (2013) Beamforming of joint polarization-space matched filtering for conformal array. The Scientific World Journal Article ID 589675, 10
23. Zou Y, Xie H, Wan L, Han G (2015) High accuracy frequency and 2d-DOAs estimation of conformal array based on PARAFAC. Journal of Internet Technology 16(1):107–119
24. Li R, Xu L, Shi XW, Chen L, Cui CY (2012) Two-dimensional NC-music DOA estimation algorithm with a conformal cylindrical antenna array. J Electromagn Waves Appl 25(5-6):805–818
25. Zou Y, Xie H, Wan L, Han G, Li W (2015) 2D-DOA and mutual coupling estimation in vehicle communication system via conformal array. Mobile Information Systems Article ID 841341, 10
26. Qi ZS, Guo Y, Wang BH (2011) Blind direction-of-arrival estimation algorithm for conformal array antenna with respect to polarisation diversity. IET Microw Antennas Propag 5(4):433–442
27. Si WJ, Wan LT, Tian ZX (2013) Fast DOA estimation based on cylindrical conformal array antenna. Syst Eng Electron 35(8):1589–1595
28. Howland PE, Griffiths HD, Baker CJ (2008) Passive bistatic radar systems Bistatic radar: emerging technology. Wiley, New York